

pubs.acs.org/JCTC Article

DFT + F12 QFFs for Cost-Effective Rovibrational Spectral Data Predictions of Ground and Excited Electronic States

Noah R. Garrett, Megan C. Davis, and Ryan C. Fortenberry*



Cite This: J. Chem. Theory Comput. 2024, 20, 1324–1336



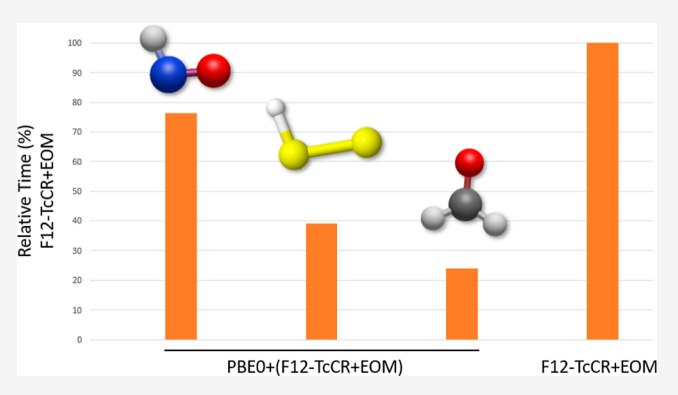
ACCESS I

III Metrics & More

Article Recommendations

SI Supporting Information

ABSTRACT: The quest for faster computation of anharmonic vibrational frequencies of both ground and excited electronic states has led to combining coupled cluster theory harmonic force constants with density functional theory cubic and quartic force constants for defining a quartic force field (QFF) utilized in conjunction with vibrational perturbation theory at second order (VPT2). This work shows that explicitly correlated coupled cluster theory at the singles, doubles, and perturbative triples levels [CCSD(T)-F12] provides accurate anharmonic vibrational frequencies and rotational constants when conjoined with any of B3LYP, CAM-B3LYP, BHandHLYP, PBE0, and ω B97XD for roughly one-quarter of the computational time of the CCSD(T)-F12 QFF alone for our test set. As the number of atoms in the



molecule increases, however, the anharmonic terms become a greater portion of the QFF, and the cost comparison improves with HOCO⁺ and formic acid, requiring less than 15 and 10% of the time, respectively. In electronically excited states, PBE0 produces more consistently accurate results. Additionally, as the size of the molecule and, in turn, QFF increase, the cost savings for utilizing such a hybrid approach for both ground- and excited-state computations grows. As such, these methods are promising for predicting accurate rovibrational spectral properties for electronically excited states. In cases where well-behaved potentials for a small selection of targeted excited states are needed, such an approach should reduce the computational cost compared to that of methods requiring semiglobal potential surfaces or variational treatments of the rovibronic Hamiltonian. Such applications include spectral characterization of comets, exoplanets, or any situation in which gas phase molecules are being excited by UV—vis radiation.

1. INTRODUCTION

Excitations into electronic states higher than the ground state are often thought of as simply moving the electron from an occupied molecular orbital (MO) to a previously unoccupied MO. While such an approximation is most often convenient and somewhat accurate enough for making connections from theory to experiment, the shift of that orbital occupation can exhibit significant geometric effects and changes in the molecular properties of the molecule. Most notably, the strength of the bonds must change as a result of an electron moving out of a "bonding" orbital or into an "anti-bonding" orbital or both. This change of bond strength then influences the length of the bonds, the positions of the atoms, the rotational constants, and the vibrational frequencies among other structural and spectroscopic considerations. Many of the vibrational frequencies of large molecules may not change significantly. However, some differences must be present due to nuclei response to the change of electronic wave function. In the case of the vibrational frequencies, in large molecules, many, if not most, of the fundamental vibrational frequencies may be unchanged, but the different electronic wave function must create some differences in the way in which the nuclei respond to the shift in electronic structure. While this nuclear response is often not needed for the electronic spectral implications being modeled, applications such as high-resolution spectroscopy, remote telescopic observations of comets^{1,2} or exoplanets,³ and the development of next-generation solar energy harvesting materials where the vibronic or even rovibronic spectra must be characterized are at an extreme disadvantage as few currently available theoretical approaches are able to treat vibrational behavior anharmonically.

In most cases where electronically excited states require vibrational frequency characterization, the harmonic approximation is sufficient. However, highly accurate rovibronic spectra require greater accuracy from the anharmonic potentials. This level of accuracy is necessary to provide high-resolution spectra, which have many applications

Received: October 24, 2023 Revised: January 3, 2024 Accepted: January 3, 2024 Published: January 17, 2024





including the analysis of cometary spectra.¹ Anharmonic vibrational frequencies are commonly computed for ground electronic states to accuracies bordering on the 1 cm⁻¹ spectroscopic accuracy range, 4-9 but these often rely upon composite schema and/or coupled cluster theory at the singles, doubles, and perturbative triples levels [CCSD(T)]¹⁰ known for their balance of accuracy with time cost. 11 Since the CCSD(T) energy is formed in a perturbative fashion, and no CCSD(T) wave function is created per se, its direct application to nonvariationally accessible electronic states is not possible. Within coupled cluster theory, the equation of motion formalism¹² is most commonly utilized to treat electronically excited states. However, equation-of-motion (EOM)-CCSD is not accurate enough for the computation of anharmonic vibrational frequencies, 13 and most triples methods are too slow, especially EOM-CCSDT. Even the iterative, approximate triples EOM-CC3¹⁴⁻¹⁶ is not efficient enough to emulate the sweet spot that CCSD(T) provides in ground electronic states. While some EOM-CCSD(T) and related perturbative methods exist, 18 none have risen to the top for community usage the way that CCSD(T) did in its first decade and beyond. Active work in our group is exploring the use of CCSD(T)(a)*, which should alleviate many of these issues, 19 but this is still in development. Beyond these and furthermore, multireference configuration interaction computations can access any electronic state desired in principle and have been utilized to compute anharmonic vibrational frequencies.²⁰ However, inconsistencies resulting from the choice of active space and the growth of the computational cost from the static correlation make them less than desirable for generic use in this application.²¹

Several composite methods have been proposed in our group of late to address this issue. 22-25 These most often utilize EOM-CCSD for the excited-state computation but are conjoined to some CCSD(T) definition of the ground electronic state. While full EOM-CCSDT methods²⁶ with considerations for complete basis set (CBS) extrapolations ("C") and core electron correlation ("cC") provide accurate descriptions in the so-called EOM-CCSDT-CcC approach, 27 they are prohibitively time-consuming for all but the smallest molecules. The use of explicitly correlated approaches in CCSD(T)-F12b in the ground electronic state combined with EOM-CCSD for the excited state with the addition of scalar relativity ("R") to the CcC considerations shows promise in the F12-TcCR + EOM methodology, which reports mean absolute percent differences (MA%Ds) compared to gas phase experiment of less than 2.5%. Here, the CBS extrapolation is not utilized as the basis is truncated simply at the triple- ζ level ("T") due to the faster CBS convergence of F12.²⁸ While faster than canonical coupled cluster approaches, this method is still likely not going to contribute to the computation of electronically excited vibrational spectra for molecules of more than six or so atoms. Since the size of the typical anharmonic potential grows geometrically with the number of atoms and the computational cost of each single point computation grows polynomially with the number of electrons, faster methods are needed.

Most anharmonic vibrational frequencies reported in the literature are computed via quartic force fields (QFFs), fourthorder Taylor series approximations of the internuclear Watson Hamiltonian^{9,29,30}

$$V = \frac{1}{2} \sum_{ij} F_{ij} \Delta_i \Delta_j + \frac{1}{6} \sum_{ijk} F_{ijk} \Delta_i \Delta_j \Delta_k$$
$$+ \frac{1}{24} \sum_{ijkl} F_{ijkl} \Delta_i \Delta_j \Delta_k \Delta_l$$
(1)

The terms $F_{ij...}$ represent the force constants. The terms $\Delta_i \Delta_j$... are the displacements for coordinates *i*, *j*, etc.

The harmonic approximation is the first of the QFF terms in eq 1, and the cubic and quartic terms are added to the definition of the potential. As such, a different approach to speeding up anharmonic vibrational frequency computations utilizing QFFs is to treat the harmonic terms at higher level and the remaining terms with lower-level methods. 5,31-34 Such an approach capitalizes on the nature of QFFs since the harmonic portion requires the least amount of computational power meanwhile producing the majority of the accuracy in calculating the fundamental frequency.⁸ While some works^{5,32-35} have highlighted success in doing so for ground electronic states, the present work will further benchmark such approaches and will extend it to electronically excited states, as well. The present work will apply this technique to both electronic ground and excited states by utilizing F12-TcCR and F12 + EOM, respectively, for the harmonic terms in eq 1 and a testbed of density functional theory (DFT) methods for the anharmonic corrections, giving what will be called the DFT + F12 QFF approach. The functionals are chosen on the basis of popularity and robustness of these functionals for the chemical moieties present in the set of molecules used for benchmarking. The aim is not only to retain accuracy for predicting rovibronic spectral features utilizing the sparse QFF potential but also to decrease the computational time in a manner that can support the computation of rovibronic spectral properties for molecules containing on the order of 10 or more atoms. Additionally and in working toward such an aim, this work will provide predictions for vibrational frequencies and spectroscopic constants of nonvariationally accessible electronic states of two molecules of importance to atmospheric chemistry and astrochemistry, protonated carbon dioxide as well as for formaldehyde, that have not been experimentally characterized

2. COMPUTATIONAL METHODS

DFT + F12 QFFs are utilized in this work to efficiently compute the anharmonic vibrational frequencies and rotational constants for both ground state and electronically excited states of a test set of molecules chosen for their available reference data utilized in previous work. 24,25 The F12 portion for ground electronic states is built upon the F12-TcCR approach based on CCSD(T)-F12b at a triple-\(\zeta \) basis level ("T") along with the corresponding core correlation ccpCVTZ-F12 basis set ("cC"). 8,36,37 For further accuracy improvements, the Douglas-Kroll formalism³⁸ within canonical CCSD(T) is implemented as a composite term within the single-point energy to account for scalar relativistic effects ("R"). Again, the F12-TcCR + EOM approach is a composite method that relies upon CCSD(T)-F12b energies for the reference, ground-state energies, and EOM-CCSD for the excitation energies. Within the DFT + F12 approach, the F12-TcCR approach is further coupled with DFT for computations of ground-state properties, while the F12-TcCR + EOM approach is combined with time-dependent DFT (TD-DFT) for excited states. For the DFT methods, several common

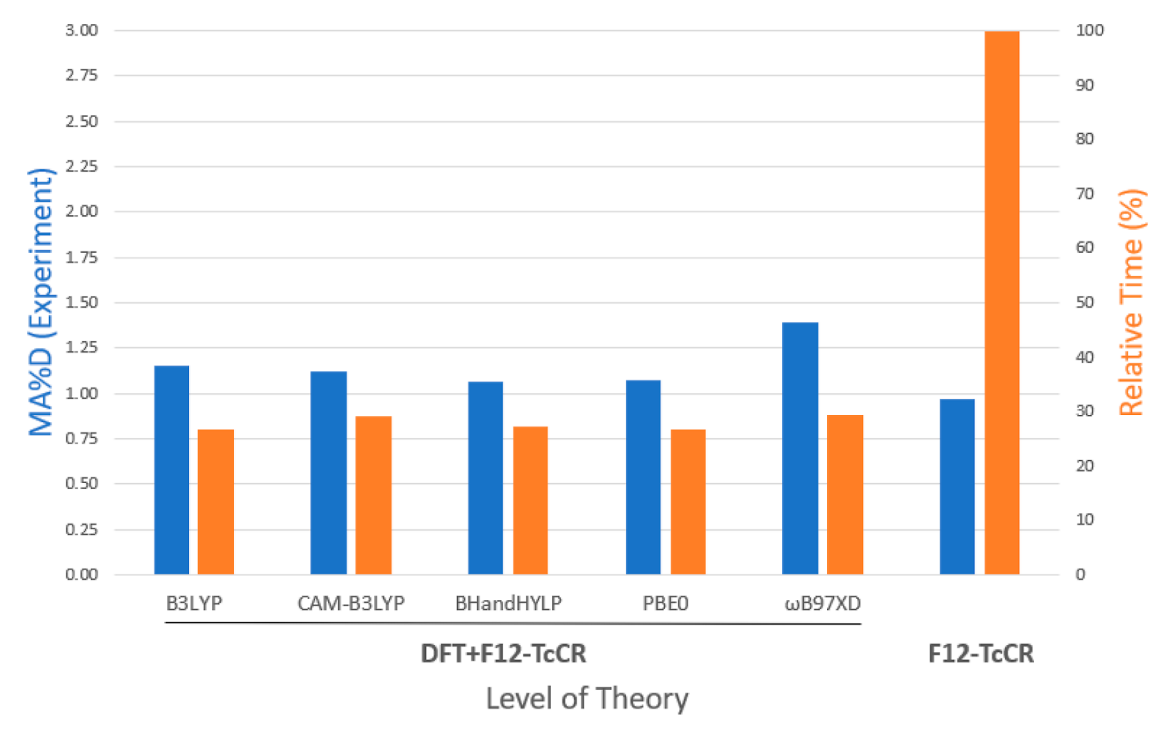


Figure 1. MA%Ds and relative times (%) for ground-state anharmonic frequencies related to experiment (cm⁻¹) with DFT + F12-TcCR.

functionals including B3LYP, CAM-B3LYP, BHandHLYP, PBE0, and ω B97XD³⁹⁻⁴⁵ are chosen in order to compare the difference in accuracy between each functional when combined with F12-TcCR and F12-TcCR + EOM. The DFT methods exclusively employ the aug-cc-pVTZ basis set. ^{46,47} All open-shell molecules employ restricted open-shell references. 48–50

All QFFs utilize step sizes of 0.005 Å for bond lengths and 0.005 radians for bond angles in each molecule's respective symmetry-internal coordinate system to produce the single points needed for defining the QFF. All coupled cluster computations utilize Molpro2022, 51,52 and all DFT computations employ Gaussian 16.53 Each QFF is fit via a least-squares procedure to generate tight fittings of the energies for any level of theory with a sum of residuals squared that should be on the order of 10⁻¹⁶ a.u.² or better, but some on the order of 10⁻¹³ a.u.2 or better still produce stable enough potential surfaces for further use. 7,54 The full DFT QFF is computed for each molecule and each electronic state of interest. After the DFT QFF is computed and fit, the force constants for the latter two terms of eq 1 are conjoined to the coupled cluster theory harmonic terms in both symmetry-internal coordinates to produce the utilized QFF for the hybrid DFT + F12 methodology.

The resulting QFF utilizing coupled cluster harmonic terms and DFT anharmonic terms is then fed into a second-order vibrational perturbation theory (VPT2) code called PBQFF written in the modern Rust programming language built upon the previous FORTRAN77 SPECTRO code. 55,56 This produces the anharmonic fundamental vibrational frequencies and the rotational constants utilized for comparison to the experimental benchmarks: NH₂⁻, HNO, HOO, HNF, HSO, HSS, H₂CO, HOCO⁺, and formic acid. The HNO, HOO, HNF, HSO, and HSS F12-TcCR + EOM excited-state harmonic force constants are from ref 27. The performance of each method's frequencies and rotational constants are evaluated as

MA%Ds compared to experiment. These are averages over the total number of vibrational frequencies or rotational constants treated as individual items and are not averages over the number of molecules. Due to the relatively large numbers of results, the vibrational frequencies are listed in decreasing frequency order instead of standard Herzberg ordering.

3. RESULTS AND DISCUSSION

3.1. DFT + **F12 Ground Electronic States.** The performance of the DFT + F12 hybrid QFFs is most succinctly given in Figure 1 for the ground electronic states. Clearly, pure F12-TcCR QFF VPT2 results are the most accurate (black bars) but are also the slowest (orange bars); F12-TcCR is the time benchmark and is given as 100%. The specific accuracies for the various DFT functionals are given in Table 1 including both the individual vibrational frequencies of each molecule analyzed and the averages correlating to the black bars in Figure 1. The individual timings are given in Table 2.

From Figure 1 and Table 2, the chosen five functionals all give timings that are nearly identical at slightly more than a quarter of the time taken to compute full F12-TcCR QFFs. The significant reduction in computational time is sensible as DFT scales ostensibly as $O(N^4)$ and CCSD(T)-F12 as $O(N^7)$. However, and in line with similar hybrid approaches, 35 the speedup increases significantly as the size of the number of atoms in the molecule grows due to the greater increase in the number of anharmonic terms in the QFF versus the harmonic terms. For instance, from Table 2, NH₂⁻ has 16 harmonic points out of the total 69 points, which only reduces time by only about two-thirds, but HOCO+ has 61 harmonic points out of the total 743 points, leading to a time reduction of around one-eighth of the cost. Formic acid has some aberrations in the B3LYP and ω B97XD functionals, where the fittings were poor. In any case, DFT + F12-TcCR groundstate QFFs promise to decrease the computational time notably allowing for larger molecular systems to be analyzed.

Table 1. MA%Ds for Ground-State Anharmonic Vibrational Frequencies Relative to Experiment (cm^{-1}) with DFT + F12-TcCR

			D						
molecule	mode	B3LYP	CAM-B3LYP	BHandHLYP	PBE0	ωB97XD	F12-TcCR	experiment	ref.
$\mathrm{NH_2}^-$	$ u_1 $	0.31	0.06	1.06	0.02	0.23	0.13	3190.291	57
$\mathrm{NH_2}^-$	$ u_2$	0.41	0.03	0.90	0.14	0.33	0.22	3121.9306	57
HNO	$ u_1$	1.67	1.67	1.33	1.27	0.97	0.46	2683.9521	58
HNO	$ u_2$	0.61	0.61	0.07	0.38	0.41	0.76	1565.3481	58
HNO	$ u_3$	0.77	0.76	0.17	0.62	0.63	0.84	1500.8192	58
НОО	$ u_1$	1.19	1.02	0.47	0.75	0.42	0.34	3436.1951	59
НОО	$ u_2$	0.83	0.70	0.43	0.65	0.64	0.61	1391.75442	59
НОО	$ u_3$	2.28	1.78	1.12	1.55	1.25	1.90	1097.62598	59
HNF	$ u_1$	0.32	0.07	1.09	0.06	0.10	0.45	3167	60
$HNFNH_2$	$ u_2$	0.15	0.24	0.47	0.31	0.34	0.30	1439	60
HNF	$ u_3$	0.77	0.28	0.29	0.06	0.25	0.29	1015	60
HSO	$ u_1$	1.58	1.04	0.03	1.32	0.46	0.50	2325.1	61
HSO	$ u_2$	2.36	2.17	1.90	2.34	1.18	1.50	1080.4	61
HSO	$ u_3$	1.33	1.14	0.93	1.62	1.45	1.94	1013.9	61
HSS	$ u_1$	6.89	7.23	7.79	7.05	5.93	7.55	2688	62
HSS	$ u_2$	1.48	1.53	1.44	0.91	8.32	0.98	892	62
HSS	$ u_3$	0.89	0.69	0.64	0.56	1.24	0.52	596.27996	62
H_2CO	$ u_1$	0.70	0.59	0.02	0.70	0.95	0.20	2843.1	63-65
H_2CO	$ u_2$	0.40	0.28	0.52	0.41	0.12	0.10	2782.5	63-65
H_2CO	$ u_3$	0.25	0.14	0.21	0.14	0.20	0.26	1746.1	63-65
H_2CO	$ u_4$	0.77	0.75	0.44	0.75	0.79	0.55	1500.1	63-65
H_2CO	$ u_5$	0.52	0.52	0.42	0.61	1.60	0.28	1249.1	63-65
H_2CO	$ u_6$	0.93	0.90	0.76	0.96	3.25	0.21	1167.3	63-65
HOCO+	$ u_1$	0.69	0.66	0.32	0.43	1.92	0.34	3375.37413	66,67
HOCO+	$ u_2 $	0.63	0.75	1.02	0.67	1.78	0.43	2399	68
нсоон	$ u_1$		0.48	0.71	0.23		0.27	3570.5	63-65
нсоон	$ u_2$		0.18	0.54	0.25		0.15	2942.06	63-65
нсоон	$ u_3$		0.68	0.36	0.68		0.79	1776.8334	63-65
нсоон	$ u_4$		0.26	0.07	0.24		0.08	1379.05447	63-65
нсоон	ν_5		8.27	8.03	8.27		8.00	1220.8	63-65
нсоон	$ u_6$		0.06	0.38	0.02		0.25	1104.8521	63-65
НСООН	$ u_7$		0.41	0.52	0.47		0.33	626.1656	63-65
НСООН	$ u_8$		0.96	0.79	0.99		0.61	1033	63-65
НСООН	ν_9		1.09	0.95	1.18		0.78	640.7251	63-65
average		1.15	1.12	1.06	1.08	1.39	0.97		

Table 2. Timing as a Percentage of the F12-TcCR Wall Time (%)

			DFT + F12-TcCR			
molecule	B3LYP	CAM-B3LYP	BHandHLYP	PBE0	ω B97XD	Harm./total Pts
NH 2	66.6	71.7	67.2	66.0	76.2	16/69
HNO	26.6	33.5	28.5	26.4	30.1	24/129
НОО	21.4	21.9	21.6	21.5	22.2	24/129
HNF	21.0	21.4	21.3	21.0	21.7	24/129
HSO	19.6	19.9	19.7	19.6	19.8	24/129
HSS	19.1	19.3	19.1	19.1	19.3	24/129
H_2CO	22.7	29.6	22.9	23.0	30.2	34/413
HOCO+	13.3	16.2	13.5	13.3	16.6	61/743
НСООН	8.1	28.4	9.2	9.1	25.8	180/5641
average	26.8	29.1	27.3	26.7	29.4	

In digging past Figure 1 for the accuracies in Table 1, the F12-TcCR QFFs produce errors compared to the experiment of just under 1%. The DFT + F12-TcCR values are slightly higher ranging from 1.06 to 1.39%. However, for speedups of approaching 90%, such errors are certainly acceptable. Most of the functionals are also giving similar anharmonic behavior for specific fundamentals. For instance, the ν_1 S-H stretch in HSS

has an error of 7.55% from F12-TcCR, which is the highest of the test set. The error of this same fundamental fluctuates from 5.93% with ω B97XD producing the anharmonic terms to 7.79% with BHandHLYP. Hence, no variance between functionals is greater than $\pm 2\%$; most are within 0.5% or less, showing that the anharmonic corrections (which themselves are on the order of 2–5% regardless of the

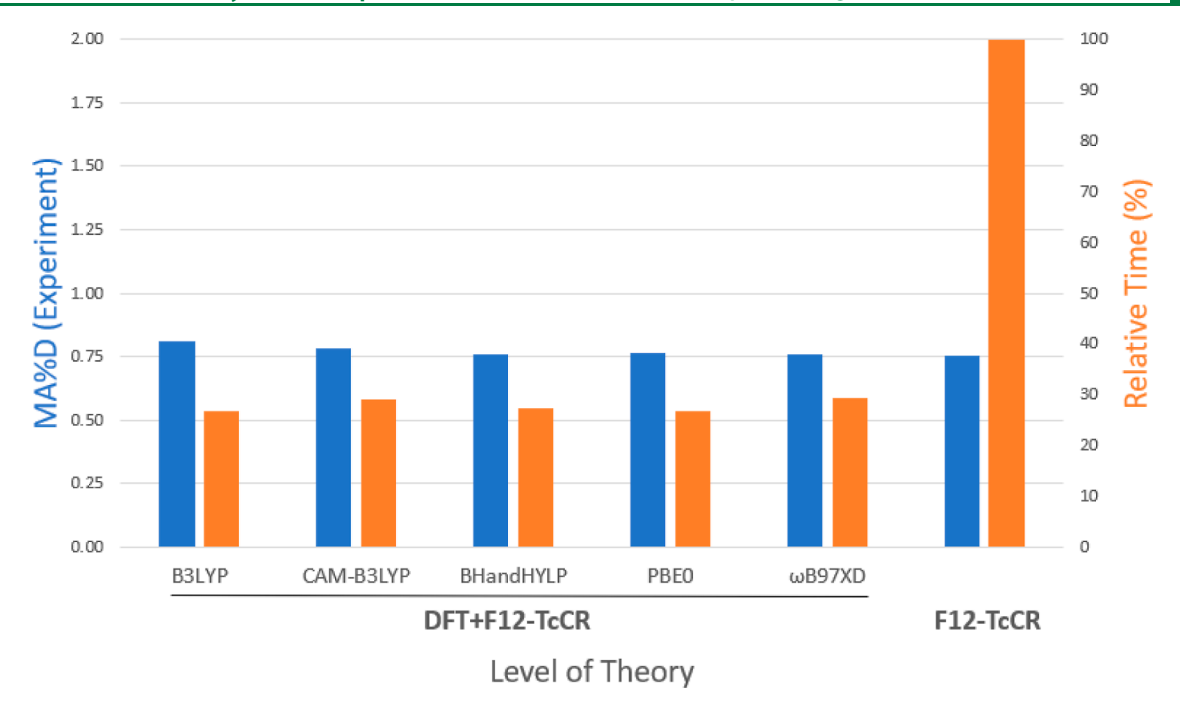


Figure 2. MA%Ds and relative times (%) for ground-state rotational constants related to experiment (MHz) with DFT + F12-TcCR.

electronic structure method) that are produced by the DFT portions of the hybrid QFF are both essential and consistent for computing such properties.

The performance of the ground electronic states' rotational constants also behaves in a similar fashion as shown in Figure 2 and Table 3. F12-TcCR rotational constants exhibit a MA%D from experiment of 0.75% which is double the error of pure coupled cluster approaches, 8,35 but is more than acceptable for the speed-up gained, especially if this opens the ability to compute data for larger molecules. The vibrational states for each rotational constant are denoted in Table 3 as subscripts (i.e., vibrational state i to give the rotational constant A_i), and these are computed from an R_{α} -averaged anharmonic procedure. The various functionals in the DFT + F12-TcCR perform effectively in the same error, again since most of the rotational constant value is a product of the F12-TcCR minimum geometry. All of the functionals produce rotational constants within 0.5% or less of one another save for some of the A constants of the more prolate molecules.

Once more, there is no clear best choice for functional to include in this hybrid QFF. All are producing roughly similar results. PBE0 generates the lowest error for fundamental vibrational frequencies, the second-lowest for rotational constants, and the second-lowest average time and does not experience convergence issues for formic acid the way that B3LYP and ω B97XD do. Numerical instabilities arise for these functionals in the symmetry-breaking (out-of-plane) coordinates producing nonsensical results that could not be rectified, leading to their exclusion in the formic acid data set. Hence, if one functional has to be recommended from this set, it would likely be PBE0 (giving the PBE0 + F12-TcCR QFF), but the choice of any functional appears to produce nearly identical results for inclusion in ground-state hybrid DFT + F12-TcCR QFFs.

3.2. DFT + **F12 Electronically Excited States.** The electronically excited states, however, are much more variable, especially in terms of accuracy, as shown in Figure 3 and Table 4 but still have promising predictive power in modeling the

rovibrational structure of electronically excited states. The MA %D for any of the DFT + (F12-TcCR + EOM) and pure F12-TcCR + EOM methods is also much larger across the board well above 2%, double or more what the ground-state hybrid QFF can produce. Furthermore, the timing is also more variable but does not produce as much speedup as the ground-state QFF inclusion of DFT provides (Table 5). The TD portion of a TD-DFT computation represents the vast majority (more than 80%) of the computation, and this contributes to the seemingly lower returns for the excited-state hybrid QFF timings.

Even so, all is certainly not lost. The biggest reason for the statistics is, once more, the product of our test set. Since small molecules have more complete sets of reference data and provide for larger numbers of data points to be computed, they skew the results. Table 5 shows that the triatomic molecules in this study have at least two heavy atoms and generate timings of roughly 100% or less of the F12-TcCR + EOM. The DFT + (F12-TcCR + EOM) HSS radical QFFs are roughly 40% of the F12-TcCR + EOM QFF timings for the various functionals, implying that the $O(N^4)$ TD-DFT approach is still giving useful speedup in the computation. Furthermore, the tetratomic formaldehyde and protonated carbon dioxide are much less than this. While inclusion of CAM-B3LYP and ω B97XD as the anharmonic terms produces slower QFFs than the other three functionals, the others are on the order of 40% or less compared to the coupled cluster results. Consequently, the larger the molecule, the more benefit the hybrid DFT + F12 QFF generates.

In terms of accuracy, F12-TcCR + EOM still is the most accurate, with a MA%D of 2.52%. However, the corrections from B3LYP and PBE0 are close at 3.54 and 3.87%. While BHandHLYP and ω B97XD are at 9.23 and 16.88%, respectively, compared to the experimental benchmarks, CAM-B3LYP is much less as given in Table 4. The errors are once more related most closely to the harmonic computations from F12-TcCR + EOM. Hence, when F12-

Table 3. MA%Ds for Ground-State Rotational Constants Relative to the Experiment (MHz) with DFT + F12-TcCR

			D						
molecule	Const.	B3LYP	CAM-B3LYP	BHandHLYP	PBE0	ω B97XD	F12-TcCR	experiment	re
NH_2^-	A_0	0.59	0.72	1.02	0.68	0.64	0.69	691 045.5991	57
NH_2^-	B_{0}	0.32	0.28	0.16	0.29	0.31	0.32	391 780.7758	57
NH_2^-	C_0	0.12	0.04	0.16	0.06	0.09	0.08	243 270.4873	57
NH_2^-	A_1	1.24	1.50	2.19	1.38	1.32	1.35	660 976.4155	57
NH_2^-	B_1	0.53	0.43	0.21	0.43	0.49	0.49	389 361.4507	57
NH_2^-	C_1	0.20	0.05	0.36	0.09	0.15	0.14	239 134.5506	57
NH_2^-	A_2	0.72	1.03	1.61	0.90	0.83	0.85	670 908.5397	57
NH_2^-	B_2	0.34	0.28	0.02	0.28	0.33	0.33	386 159.6672	57
NH_2^-	C_2	0.15	0.00	0.39	0.04	0.10	0.09	238 082.2791	57
INO	A_0	1.47	1.47	0.97	1.40	1.36	1.11	553 898.62	58
INO	B_0	0.13	0.13	0.03	0.09	0.10	0.18	42 312.81245	58
INO	C_0	0.18	0.18	0.05	0.13	0.14	0.20	39 165.14154	58
INO	A_1	2.58	2.58	4.06	2.77	2.90	3.59	553 898.62	58
HNO	B_1	0.54	0.54	0.49	0.50	0.53	0.62	42 312.8124	58
INO	C_1	0.40	0.40	0.25	0.35	0.37	0.41	39 165.1415	58
INO	A_2	1.57	1.57	1.07	1.50	1.47	1.21	556 822.25	58
INO	B_2	0.11	0.11	0.14	0.01	0.03	0.21	42 009.1077	58
INO	C_2	0.95	0.95	0.69	0.85	0.87	1.02	38 945.43863	58
INO	A_3	1.51	1.51	1.01	1.42	1.40	1.08	564 254.9744	58
INO	B_3	0.05	0.05	0.23	0.13	0.11	0.04	42 271.33616	58
INO	C_3	0.62	0.62	0.83	0.71	0.68	0.57	38 716.99678	58
Ю	A_0	1.40	1.35	1.06	1.29	1.23	1.20	610 273.2246	69
Ю	B_0	0.53	0.43	0.32	0.41	0.38	0.45	33 517.8161	69
Ю	C_0	0.55	0.46	0.34	0.43	0.41	0.47	31 667.65414	69
ЮО	A_1	1.81	1.63	0.69	1.51	1.30	1.25	587 118	59
ЮО	B ₁	0.43	0.32	0.20	0.32	0.29	0.32	33 649	59
100	C_1	0.51	0.39	0.24	0.39	0.35	0.38	31 725.5	59
100 100	A_2	1.41	1.39	1.21	1.31	1.27	1.13	628 297.3588	69
100 100	B_2	0.53	0.43	0.32	0.39	0.37	0.44	33 464.33312	69
100 100	C_2	0.59	0.49	0.38	0.45	0.43	0.49	31 484.80352	69
100	A_3	1.45	1.35	1.02	1.25	1.20	1.23	608 855.1883	69
100	B ₃	0.66	0.39	0.08	0.30	0.24	0.46	33 144.75436	69
100	C_3	0.70	0.44	0.13	0.36	0.29	0.50	31 258.46022	69
INF	A_0	0.70	0.18	0.07	0.30	0.18	0.07	530 272.90	70
INF	B_0	0.47	0.39	0.30	0.17	0.13	0.38	31 145.44	70
INF		0.50	0.41	0.31	0.38	0.40	0.38	29 310.71	70
INF ISO	C_0	0.30	0.23	0.05	0.38	0.40	0.40	299 483.9	61
	A_0								
HSO HSO	B_0	0.49	0.45	0.41	0.45	0.43	0.35	20 502.7847	61
	C_0	0.47	0.43	0.38	0.43	0.41	0.33	19 135.6989	61
HSS HSS	A_0	0.45	0.38	0.27	0.42	0.30	0.29	296 978.9619	62
ISS ISS	B_0	0.10	0.07	0.07	0.05	0.06	0.05	7996.36601	62
HSS L CO	C_0	0.11	0.08	0.07	0.06	0.07	0.05	7776.73845	62
H₂CO	A_0	0.36	0.34	0.11	0.36	0.34	0.25	281 970.5406	71
H ₂ CO	B_0	0.93	0.94	0.98	0.94	0.94	0.94	38 836.05038	71
I₂CO	C_0	0.77	0.79	0.85	0.79	0.79	0.80	34 002.19978	71
HOCO ⁺	A_0	3.56	3.58	3.73	3.66	3.67	3.51	789 938.5	66,
HOCO+	B_0	1.10	1.11	1.16	1.11	1.12	1.07	10773.636	66,
HOCO+	C_0	1.11	1.13	1.17	1.12	1.13	1.08	10 609.502	66
HOCO+	\mathbf{A}_1	3.92	3.96	4.64	4.19	4.39	4.07	755 878.2	66
HOCO+	\mathbf{B}_1	1.07	1.09	1.14	1.09	1.10	1.05	10 761.222	66
HOCO⁺	C_1	1.08	1.10	1.16	1.10	1.11	1.05	10 589.765	66
НСООН	A_0	0.11	0.15	0.27	0.16	0.03	0.17	77 510.7404	65
НСООН	B_{0}	0.95	0.98	1.03	0.97	1.13	0.97	12 054.9545	65
НСООН	C_0	0.84	0.87	0.94	0.87	0.99	0.87	10 416.289	65
verage		0.81	0.78	0.76	0.77	0.76	0.75		

TcCR + EOM is in error, this is consistently transferred to the DFT + EOM QFF results as well. One notable exception is BHandHLYP and ω B97XD for the \tilde{A}^1A'' state of H₂CO.

Although BHandHLYP can accurately describe the symmetric and antisymmetric hydride stretches, modes ν_1 and ν_2 , these functionals are not able to reproduce the full excited-state

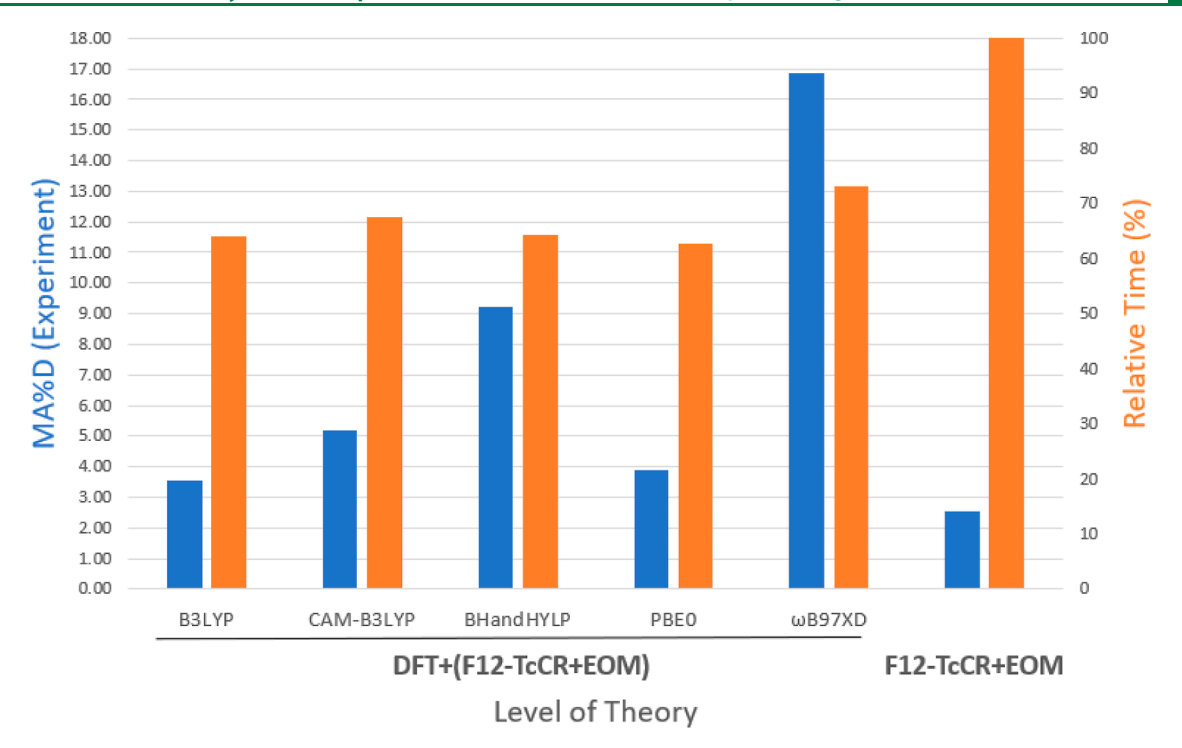


Figure 3. MA%Ds and relative times (%) for electronically excited state anharmonic frequencies related to experiment (cm^{-1}) with DFT + (F12-TcCR + EOM).

Table 4. MA%Ds for Electronically Excited State Anharmonic Vibrational Frequencies Relative to Experiment (cm⁻¹) with DFT + (F12-TcCR + EOM)

DFT + (F12-TcCR + EOM)									
molecule	mode	B3LYP	CAM-B3LYP	BHandHLYP	PBE0	ω B97XD	F12-TcCR + EOM	experiment	ref.
HNO	$ u_1$	1.74	7.56	6.00	1.19	1.50	1.78	2854.17	72
HNO	$ u_2$	1.78	0.25	0.79	1.12	1.21	2.34	1420.77	72,73
HNO	$ u_3$	2.35	4.32	4.67	5.35	3.84	0.46	981.18	72,73
HOO	$ u_1$	9.42	9.66	8.20	8.85	8.45	8.28	3268.5	74
НОО	$ u_2 $	5.87	7.91	8.21	6.52	6.23	9.84	1285	74
HOO	$ u_3$	1.53	4.75	6.42	0.11	0.78	0.08	929.068	74-7576
HNF	$ u_2$	8.49	9.09		1.41	1.63	1.81	1121	77
HNF	$ u_3$	3.06	21.18		0.75	1.32	0.45	1074	77
HSO	$ u_1$	8.26	9.18	9.40	8.38	6.10	8.81	2769	78
HSO	$ u_2$	1.01	6.23	3.89	0.83	8.45	0.76	828	78
HSO	$ u_3$	1.25	2.29	1.54	0.90	1.10	1.70	702	78
HSS	$ u_1$	0.85	0.69	0.27	0.32	1.65	0.45	2550	79
HSS	$ u_2$	6.93	6.92	6.66	7.82	0.09	6.72	808	62
HSS	$ u_3$	0.27	0.33	0.19	1.42	0.43	0.23	504.533914	62
H_2CO	$ u_1$	0.27	0.42	2.32	0.43	33.45	0.48	2968	80
H_2CO	$ u_2$	1.07	0.53	0.69	2.35	16.62	0.31	2847	80
H_2CO	$ u_4$	2.40	2.93	6.87	1.31	72.78	0.39	1293.1	81
H_2CO	$\nu_{5} + \nu_{6}$	0.14	0.33	54.85	3.48	33.86	0.39	1183 ^a	81
H_2CO	$ u_5$	10.65	3.81	35.89	20.90	121.32	2.57	904	81
average		3.54	5.18	9.23	3.87	16.88	2.52		
average ^b		3.15	5.25	7.56	2.92	11.08	2.52		

^aThe current computations have this frequency labeled as the $\nu_5 + \nu_6$ combination band. See text for more discussion. ^bAverage MA%Ds for electronically excited state anharmonic vibrational frequencies relative to experiment excluding ν_5 for the \tilde{A}^1A'' state of H₂CO.

potential surface within the QFF sufficiently. B3LYP and PBE0 also struggle to describe the ν_5 CH₂ rocking motion, producing differences of 10.65 and 20.90%. However, the ν_5 fundamental may be misassigned in ref 81. Our computations consistently have ν_5 below 900 cm⁻¹. However, the ν_5 + ν_6 combination band at 1187.6 cm⁻¹ is very close to the experimentally

observed transition at $1183~{\rm cm}^{-1}$. Shifting to this interpretation drops the MA%Ds for each method in the "b" footnoted average of Table 4.

Additionally, the ν_2 S–O stretch of A²A' HSO has significant fluctuations across the functional set producing differences ranging from 8.45% in ω B97XD to 0.83% in PBE0.

Table 5. Timing as a Percentage of the F12-TcCR + EOM Wall Time (%)

		DFT + (F12-TcCR + EOM)						
state	molecule	B3LYP	CAM-B3LYP	BHandHLYP	PBE0	ω B97XD		
Ã1A"	HNO	76.7	77.2	74.7	76.5	86.1		
$\tilde{A}2A'$	HOO	103.3	96.5	100.6	92.4	108.4		
$\tilde{A}2A'$	HNF	92.7	92.2	90.6	101.2	105.4		
$\tilde{A}2A'$	HSO	84.0	89.5	88.2	83.8	95.1		
$\tilde{A}2A'$	HSS	40.4	40.1	40.5	39.0	39.2		
Ã1A"	H ₂ CO	23.6	25.1	24.1	24.0	25.3		
$\tilde{B}1A'$	H ₂ CO	53.4	50.0	54.1	46.3	48.8		
$\tilde{A}1A''$	HOCO ⁺	38.4	70.3	40.9	38.6	77.2		
	Average	64.1	67.6	64.2	62.7	73.2		

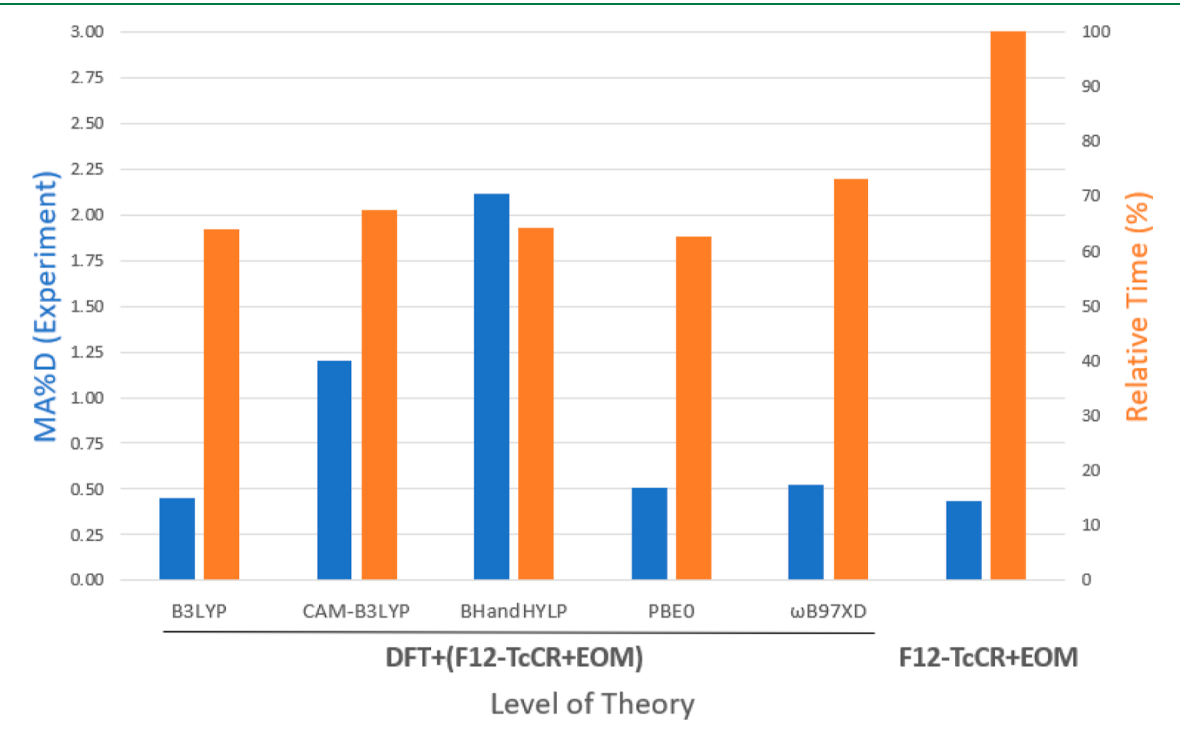


Figure 4. MA%Ds and relative times (%) for electronically excited state rotational constants related to experiment (MHz) with DFT + (F12-TcCR + EOM).

The ν_2 N–F of $\tilde{\rm A}^2{\rm A}'$ HNF also has a spike in error for CAM-B3LYP at 21.18%, but the other functionals are more consistently behaved. This excludes BHandHLYP which produces physically meaningless results prompting us to not report them in Table 4.

The ω B97XD functional redeems itself for the rotational constants as given in Figure 4 and Table 6. Its MA%D of 0.52% is not too far from that of pure F12-TcCR + EOM at 0.44%. While B3LYP is 0.45%, these errors are nearly identical for these functionals and PBE0. CAM-B3LYP produces some rotational constants notably different from the rest, increasing its MA%D, and BHandHLYP struggles to reproduce the A0 rotational constant in HNF most notably in addition to a few others giving it the largest MA%D for the rotational constants in Table 6. As such and unlike the case of the ground states, where all of the functionals were effectively producing the same performance, PBE0 appears to be the best performing functional on the whole for utilization in hybrid QFFs for electronically excited states.

3.3. Rovibrational Predictions for the \tilde{A}^1A'' and \tilde{B}^1A' States of H₂CO and \tilde{A}^1A'' State of HOCO⁺. The vibrational

frequencies and rotational constants of each fundamental are given in Table 7 for the \tilde{A}^1A'' & \tilde{B}^1A' states of H₂CO. While previous work⁸³ has termed the A state to be ¹A₂, the adiabatic state breaks $C_{2\nu}$ symmetry, creating a C_s structure with the plane of symmetry bisecting the ∠H-C-H angle. These are computed with the pure F12-TcCR + EOM QFF as well as the B3LYP and PBE0 hybrid excited-state QFFs. While the fundamental frequencies of the \tilde{A}^1A'' state (save for ν_4) are known (Table 4), the remainder of the data are produced here for comparison, and the B state is largely unexplored in the literature. 81,84 They should also be accurate to within 3.5% or less per the above benchmarks. Most notably from Table 7, the hydride stretches are consistent across the levels of theory differing by no more than 35 cm⁻¹ or less than 2%. Hydride stretches are often the most well-behaved for QFF procedures of this type^{85–87} since they often present the deepest and most clearly defined potentials. However, the other fundamental frequencies exhibit much more variance. The PBE0+(F12-TcCR + EOM) QFF is in closer agreement with the pure F12-TcCR + EOM results, but they are often different by more than 20%. The DFT + (F12-TcCR + EOM) approach is thus

Table 6. MA%Ds for Electronically Excited State Rotational Constants Relative to Experiment (MHz) with DFT + (F12-TcCR + EOM)

DFT + (F12-TcCR + EOM)									
molecule	Const.	B3LYP	CAM-B3LYP	BHandHLYP	PBE0	ωB97XD	F12-TcCR + EOM	experiment	ref.
HNO	A_0	1.12	2.94	2.45	1.50	1.38	0.75	664 460.0039	72
HNO	B_0	0.19	0.11	0.21	0.07	0.10	0.29	39 737.49031	72
HNO	C_0	0.33	0.15	0.03	0.24	0.26	0.41	37 252.21083	72
HNO	\mathbf{A}_1	1.29	5.57	4.35	1.48	1.39	1.10	620 906.1556	72
HNO	B_1	0.22	0.11	0.20	0.10	0.12	0.30	39 818.43427	72
HNO	C_1	0.58	0.49	0.34	0.47	0.49	0.64	37 120.30215	72
HNO	A_2	1.11	3.21	2.57	1.43	1.33	0.81	654 078.1911	72
HNO	B_2	0.12	0.47	0.74	0.12	0.07	0.30	39 311.78502	72
HNO	C_2	0.35	0.09	0.38	0.15	0.18	0.51	36 823.50762	72
HNO	A_3	1.26	4.07	3.41	2.56	2.17	0.02	721 330.6332	72
HNO	B_3	0.16	0.44	0.57	0.07	0.00	0.43	39 776.46333	72
HNO	C_3	0.25	0.15	0.32	0.11	0.15	0.42	37 054.34781	72
HNF	A_0	0.23	7.49	30.40	0.28	0.35	0.24	826 527.8067	77
HNF	B_0	0.29	0.40	0.41	0.21	0.24	0.29	30 965.56299	77
HNF	C_0	0.25	0.06	0.81	0.15	0.17	0.23	29 739.41183	77
HSS	A_0	0.68	0.73	0.84	0.72	0.73	0.80	289 615.1	62
HSS	B_0	0.28	0.30	0.30	0.32	0.26	0.31	7198.3	62
HSS	C_0	0.24	0.27	0.27	0.29	0.23	0.28	7011.4	62
HSS	A_3	0.63	0.69	0.80	0.67	0.69	0.76	289 500.8	62
HSS	B_3	0.16	0.25	0.24	0.33	0.16	0.26	7152.4363	62
HSS	C_3	0.16	0.24	0.24	0.32	0.16	0.25	6968.08	62
H_2CO	A_6	0.34	0.33	0.49	0.27	1.42	0.42	268 371.2105	82
H_2CO	B_6	0.44	0.36	0.31	0.38	0.34	0.57	33 693.67435	82
H_2CO	C_6	0.10	0.02	0.04	0.03	0.21	0.11	30 111.15448	82
average		0.45	1.21	2.11	0.51	0.52	0.44		

likely more valuable for accurate frequencies of hydride stretches and low-frequency bending motions but may struggle with vibrations between heavy atoms. As such, the vibrational frequencies produced by the F12-TcCR + EOM QFF alone should be taken as the most accurate, but PBE0 is likely more accurate than B3LYP.

Upon excitation into the \tilde{A} state, the mid-infrared frequencies are much more red-shifted compared to the ground state. This is exacerbated even further in the \tilde{B} state. The reason is due to the $n \to \pi^*$ and $\pi \to \pi^*$ antibonding excitations in these states. This weakens the C=O bond, which lowers the C=O stretch clearly, but it also influences the in- and out-of-plane bending as well. As such, the pure vibrational spectra of the ground state are notably different from those of either of these excited states.

The rovibrational properties for the \tilde{A}^1A'' state of HOCO⁺ are given in Table 8. None of these fundamental vibrational frequencies and rotational constants have been previously reported in the literature and may help to characterize this molecule for future laboratory examination or potential observation in cometary comae. The PBE0+(F12-TcCR + EOM) QFF is, yet again, more closely in line with the pure F12-TcCR + EOM QFF. Most notably, the ν_2 C=O stretch on the end of the molecule opposite the proton drops in frequency by nearly half to 1376.7 cm⁻¹ compared to the ground state at 2399 cm⁻¹. Hence, this $\pi \rightarrow n$ excitation significantly influences the resulting vibrational behavior of this molecule. The ν_1 O–H stretch drops by roughly 100 cm⁻¹, ^{66,67} not as much as ν_2 , but certainly enough to show explicitly that the ground-state frequencies cannot simply approximate the excited-state anharmonic frequencies. The other four fundamentals are shifting relative to their ground state values as reported in refs 7 and 85 by similar amounts as ν_1 .

4. CONCLUSIONS

The larger the molecule, the more advantage there is in using hybrid QFF approaches such as DFT + F12 reported herein. Larger molecules have a higher percentage of points in the QFF that come from the anharmonic, cubic and quartic, terms. High-level coupled cluster theory computations of the harmonic terms and DFT computations of the anharmonic terms represent nearly the extreme end of how these can be combined. This work shows that the choice of DFT functional does not change the performance in terms of time cost or accuracy significantly for ground electronic states. However, in computing electronically excited states, PBE0 gives the best overall performance of our tested set of common functionals with MA%D of less than 3.0% for fundamental vibrational frequencies (excluding ν_5 for the \tilde{A}^1A'' state of H_2CO) and 0.5% for rotational constants. It also gives the best predictions of such values for the ground-state method, but this effect is less pronounced. While the use of DFT methods in the excited-state QFF does not produce as much savings as it does for the ground-state QFFs, the effect of larger molecules is much more marked in that the inclusion of the lower-cost DFT anharmonic terms will open up the potential for examination of much larger molecules.

Beyond this benchmarking, the present work has also provided the fundamental vibrational frequencies for the \tilde{A}^1A'' and \tilde{B}^1A' states of H_2CO as well as the \tilde{A}^1A'' state of $HOCO^+$. The results of the antibonding excitation nature are clearly pronounced in the fundamental vibrational frequencies of both

Table 7. Reported Vibrational Frequencies (cm $^{-1}$) and Rotational Constants (MHz) for the \tilde{A}^1A'' and \tilde{B}^1A' States of H_2CO

	1	1		D.	
state	mode	hv	A	В	С
$\tilde{\boldsymbol{A}}^1\boldsymbol{A}''$		B3LYP +	(F12-TcCR +	· EOM)	
	$ u_0$	5022.9	268 434.6	34 064.4	30 431.1
	$ u_1$	2960.1	264 102.2	34 128.7	30 529.8
	$ u_2$	2877.5	263 250.1	34 126.3	30 483.8
	$ u_3$	1381.7	271 560.6	34 256.2	30 414.8
	$ u_4$	1262.1	268 015.0	33 648.0	30 105.6
	$\nu_5 + \nu_6$	1181.4	279 086.9	34 022.9	30 069.8
	$ u_5$	807.7	280 061.1	34 247.0	30 356.0
	ν_6	359.1	267 460.3	33 843.1	30 142.2
$\tilde{B}^{1}A'$	$ u_0$	4945.1	249 750.8	26 077.4	24 033.8
	$ u_1 $	3059.0	247 160.0	26 116.1	24 073.2
	$ u_2$	2919.4	245 945.6	26 130.5	24 059.4
	$ u_3$	1148.5	250 513.9	26 005.2	23 912.8
	$ u_4$	990.1	255 385.7	26 042.3	23 962.2
	ν_5	889.5	248 223.2	25 752.6	23 684.6
	ν_6	515.4	251 084.5	24 947.7	23 031.8
$\tilde{A}^1A^{\prime\prime}$		PBE0 +	(F12-TcCR + 1	EOM)	
	$ u_0$	5093.5	268 522.8	34 044.1	30 415.6
	$ u_1$	2955.1	264 268.1	34 109.8	30 515.6
	$ u_2$	2913.9	263 467.8	34 106.0	30 467.7
	ν_3	1670.3	271 691.1	34 234.0	30 401.6
	$ u_4$	1276.1	268 076.8	33 584.7	30 053.3
	$\nu_5 + \nu_6$	1141.8	279 128.3	34 005.2	30 057.6
	$ u_5$	715.1	280 015.0	34 231.7	30 349.5
	ν_6	399.7	267 636.1	33 820.4	30 121.0
$\tilde{B}^{1}A'$	$ u_0$	4989.8	250 037.6	25 934.7	23 913.0
	$ u_1$	3062.3	247 481.7	25 975.3	23 953.6
	$ u_2$	2947.0	246 297.6	25 987.9	23 939.5
	ν_3	1353.2	250 989.7	25 819.2	23 757.2
	$ u_4$	1017.9	255 716.5	25 905.7	23 843.0
	ν_5	820.6	248 602.8	25 569.2	23 529.3
	ν_6	491.6	251 519.0	24 595.6	22 735.4
${ ilde B}^1A'$		F12-TcC	R + EOM		
	$ u_0$	5002.7	268 316.3	34 095.3	30 436.3
	$ u_1$	2953.7	263 740.1	34 155.4	30 528.0
	$ u_2$	2855.9	263 068.7	34 154.6	30 482.1
	ν_3	1288.1	271 469.5	34 285.3	30 405.3
	$ u_4$	1275.1	267 989.9	33 746.0	30 166.9
	$\nu_5 + \nu_6$	1187.6	278 918.6	34 056.7	30 058.1
	ν_5	880.8	279 978.2	34 269.3	30 348.4
1	ν_6	319.0	267 256.7	33 885.5	30 143.2
\tilde{B}^1A'	$ u_0$	4927.5	249 172.2	25 906.2	23 897.3
	$ u_1 $	3045.3	246 349.5	25 928.8	23 920.5
	$ u_2$	2914.6	245 207.1	25 944.1	23 908.3
	$ u_3$	1194.4	249 403.8	25 927.1	23 849.5
	$ u_4$	1015.4	253 720.4	25 876.9	23 862.4
	ν_5	852.8	247 651.1	25 553.4	23 520.2
	ν_6	404.5	251 352.3	24 394.9	22 571.0

molecules. The heavy atom stretching frequencies are significantly reduced due to an increase in the antibonding character in formaldehyde and a decrease in the bonding character from protonated carbon dioxide. Both of these molecules are likely present in the coma of comets as they approach perihelion, and the novel rovibrational data for these three states of these two molecules will assist in the spectral

Table 8. Reported Vibrational Frequencies (cm⁻¹) and Rotational Constants (MHz) for the ùA″ State of HOCO+

mode B3LYP + (F12-TcCR + EOM) ν_0 4308.7 155 445.9 11 699.0 10 859.0 ν_1 3321.4 154 805.9 11 684.5 10 844.1 ν_2 1429.5 157 246.6 11 615.2 10 784.2 ν_3 1289.5 154 436.0 11 661.8 10 816.4 ν_4 1090.0 159 749.1 11 655.5 10 813.6 ν_5 891.2 191 803.8 11 720.8 10 893.5 ν_6 622.4 116 823.6 11 704.7 10 840.8 PBEO + (F12-TcCR + EOM) ν_0 4179.5 154 851.2 11 706.1 10 862.2 ν_1 3276.4 154 181.8 11 691.0 10 846.6 ν_2 1382.6 156 473.2 11 628.9 10 792.2 ν_3 1242.1 152 975.9 11 675.2 10 820.6 ν_4 1045.7 158 882.8 11 670.0 10 821.8 ν_5 571.5 191 353.1 11 722.7 10 892.8 <t< th=""><th></th><th>hv</th><th>A</th><th>В</th><th>С</th></t<>		hv	A	В	С					
$\begin{array}{c} \nu_1 \\ \nu_2 \\ \nu_2 \\ \nu_3 \\ 1289.5 \\ 157\ 246.6 \\ 11\ 615.2 \\ 10\ 784.2 \\ 10\ 794.2 \\ 1$	mode		B3LYP + (F12	-TcCR + EOM)						
$\begin{array}{cccccccccccccccccccccccccccccccccccc$	ν_0	4308.7	155 445.9	11 699.0	10 859.0					
$\begin{array}{cccccccccccccccccccccccccccccccccccc$	ν_1	3321.4	154 805.9	11 684.5	10 844.1					
$\begin{array}{cccccccccccccccccccccccccccccccccccc$	-	1429.5	157 246.6	11 615.2	10 784.2					
$\begin{array}{c} \nu_5 \\ \nu_6 \\ \hline \end{array} \hspace{0.2cm} 891.2 \\ \hline \hspace{0.2cm} 191803.8 \\ \hline \hspace{0.2cm} 11720.8 \\ \hline \hspace{0.2cm} 10893.5 \\ \hline \hspace{0.2cm} \nu_6 \\ \hline \hspace{0.2cm} 622.4 \\ \hline \hspace{0.2cm} 116823.6 \\ \hline \hspace{0.2cm} 11704.7 \\ \hline \hspace{0.2cm} 10840.8 \\ \hline \hspace{0.2cm} \textbf{PBE0} + (\textbf{F12-TcCR} + \textbf{EOM}) \\ \hline \hspace{0.2cm} \nu_0 \\ \hline \hspace{0.2cm} 4179.5 \\ \hline \hspace{0.2cm} 154851.2 \\ \hline \hspace{0.2cm} 11706.1 \\ \hline \hspace{0.2cm} 10862.2 \\ \hline \hspace{0.2cm} \nu_1 \\ \hline \hspace{0.2cm} 3276.4 \\ \hline \hspace{0.2cm} 154181.8 \\ \hline \hspace{0.2cm} 11691.0 \\ \hline \hspace{0.2cm} 10846.6 \\ \hline \hspace{0.2cm} \nu_2 \\ \hline \hspace{0.2cm} 1382.6 \\ \hline \hspace{0.2cm} 156473.2 \\ \hline \hspace{0.2cm} 11628.9 \\ \hline \hspace{0.2cm} 10792.2 \\ \hline \hspace{0.2cm} \nu_3 \\ \hline \hspace{0.2cm} 1242.1 \\ \hline \hspace{0.2cm} 152975.9 \\ \hline \hspace{0.2cm} 11675.2 \\ \hline \hspace{0.2cm} 10820.6 \\ \hline \hspace{0.2cm} \nu_4 \\ \hline \hspace{0.2cm} 1045.7 \\ \hline \hspace{0.2cm} 158882.8 \\ \hline \hspace{0.2cm} 11670.0 \\ \hline \hspace{0.2cm} 10821.8 \\ \hline \hspace{0.2cm} \nu_5 \\ \hline \hspace{0.2cm} 571.5 \\ \hline \hspace{0.2cm} 191353.1 \\ \hline \hspace{0.2cm} 11722.7 \\ \hline \hspace{0.2cm} 10892.8 \\ \hline \hspace{0.2cm} \nu_6 \\ \hline \hspace{0.2cm} 594.7 \\ \hline \hspace{0.2cm} 116240.7 \\ \hline \hspace{0.2cm} 11711.6 \\ \hline \hspace{0.2cm} 10843.8 \\ \hline \hspace{0.2cm} \textbf{F12-TcCR} + \textbf{EOM} \\ \hline \hspace{0.2cm} \nu_0 \\ \hline \hspace{0.2cm} 4165.0 \\ \hline \hspace{0.2cm} 154513.4 \\ \hline \hspace{0.2cm} 11717.4 \\ \hline \hspace{0.2cm} 10870.2 \\ \hline \hspace{0.2cm} \nu_1 \\ \hline \hspace{0.2cm} 3271.8 \\ \hline \hspace{0.2cm} 153819.0 \\ \hline \hspace{0.2cm} 11702.4 \\ \hline \hspace{0.2cm} 10854.6 \\ \hline \hspace{0.2cm} \nu_2 \\ \hline \hspace{0.2cm} 1376.7 \\ \hline \hspace{0.2cm} 158855.3 \\ \hline \hspace{0.2cm} 11692.5 \\ \hline \hspace{0.2cm} 10829.1 \\ \hline \hspace{0.2cm} \nu_4 \\ \hline \hspace{0.2cm} 1029.7 \\ \hline \hspace{0.2cm} 158375.7 \\ \hline \hspace{0.2cm} 11693.7 \\ \hline \hspace{0.2cm} 10839.5 \\ \hline \end{array}$	ν_3	1289.5	154 436.0	11 661.8	10 816.4					
$\begin{array}{cccccccccccccccccccccccccccccccccccc$	$ u_4$	1090.0	159 749.1	11 655.5	10 813.6					
$\begin{array}{c} \textbf{PBE0} + \textbf{(F12-TcCR + EOM)} \\ \nu_0 & 4179.5 & 154851.2 & 11706.1 & 10862.2 \\ \nu_1 & 3276.4 & 154181.8 & 11691.0 & 10846.6 \\ \nu_2 & 1382.6 & 156473.2 & 11628.9 & 10792.2 \\ \nu_3 & 1242.1 & 152975.9 & 11675.2 & 10820.6 \\ \nu_4 & 1045.7 & 158882.8 & 11670.0 & 10821.8 \\ \nu_5 & 571.5 & 191353.1 & 11722.7 & 10892.8 \\ \nu_6 & 594.7 & 116240.7 & 11711.6 & 10843.8 \\ \hline & \textbf{F12-TcCR + EOM} \\ \hline \nu_0 & 4165.0 & 154513.4 & 11717.4 & 10870.2 \\ \nu_1 & 3271.8 & 153819.0 & 11702.4 & 10854.6 \\ \nu_2 & 1376.7 & 155855.3 & 11661.4 & 10817.1 \\ \nu_3 & 1191.8 & 151708.5 & 11692.5 & 10829.1 \\ \nu_4 & 1029.7 & 158375.7 & 11693.7 & 10839.7 \\ \nu_5 & 589.9 & 191503.8 & 11722.6 & 10893.5 \\ \hline \end{array}$	ν_{5}	891.2	191 803.8	11 720.8	10 893.5					
$\begin{array}{cccccccccccccccccccccccccccccccccccc$	ν_6	622.4	116 823.6	11 704.7	10 840.8					
$\begin{array}{c ccccccccccccccccccccccccccccccccccc$		PBE0 + (F12-TcCR + EOM)								
$\begin{array}{cccccccccccccccccccccccccccccccccccc$	$ u_0$	4179.5	154 851.2	11 706.1	10 862.2					
$\begin{array}{cccccccccccccccccccccccccccccccccccc$	$ u_1 $	3276.4	154 181.8	11 691.0	10 846.6					
$\begin{array}{cccccccccccccccccccccccccccccccccccc$	$ u_2$	1382.6	156 473.2	11 628.9	10 792.2					
$\begin{array}{cccccccccccccccccccccccccccccccccccc$	$ u_3$	1242.1	152 975.9	11 675.2	10 820.6					
$\begin{array}{cccccccccccccccccccccccccccccccccccc$	$ u_4$	1045.7	158 882.8	11 670.0	10 821.8					
$ \begin{array}{cccccccccccccccccccccccccccccccccccc$	$ u_5$	571.5	191 353.1	11 722.7	10 892.8					
$\begin{array}{cccccccccccccccccccccccccccccccccccc$	$ u_6$	594.7	116 240.7	11 711.6	10 843.8					
$\begin{array}{cccccccccccccccccccccccccccccccccccc$			F12-TcC	R + EOM						
$\begin{array}{cccccccccccccccccccccccccccccccccccc$	$ u_0$	4165.0	154 513.4	11 717.4	10 870.2					
$ \begin{array}{cccccccccccccccccccccccccccccccccccc$	$ u_1$	3271.8	153 819.0	11 702.4	10 854.6					
$ \begin{array}{cccccccccccccccccccccccccccccccccccc$	$ u_2$	1376.7	155 855.3	11 661.4	10 817.1					
ν_{5} 589.9 191 503.8 11 722.6 10 893.5	$ u_3$	1191.8	151 708.5	11 692.5	10 829.1					
	$ u_4$	1029.7	158 375.7	11 693.7	10 839.7					
ν_6 593.7 116 142.7 11 716.7 10 847.8	$ u_5$	589.9	191 503.8	11 722.6	10 893.5					
	$ u_6$	593.7	116 142.7	11 716.7	10 847.8					

characterization of such solar system bodies, providing insights into the behavior and evolution of oxygen, ^{88,89} from the dawn of the solar system until now.

ASSOCIATED CONTENT

Supporting Information

The Supporting Information is available free of charge at https://pubs.acs.org/doi/10.1021/acs.jctc.3c01179.

Individual vibrational frequencies and rotational constants for various DFT + F12 QFFs (PDF)

AUTHOR INFORMATION

Corresponding Author

Ryan C. Fortenberry — Department of Chemistry & Biochemistry, University of Mississippi, University, Mississippi 38677-1848, United States; Orcid.org/0000-0003-4716-8225; Email: r410@olemiss.edu

Authors

Noah R. Garrett – Department of Chemistry & Biochemistry, University of Mississippi, University, Mississippi 38677-1848, United States

Megan C. Davis – Theoretical Division, T-1 and Center for Nonlinear Studies, Los Alamos National Laboratory, Los Alamos, New Mexico 87545, United States; orcid.org/ 0000-0002-4038-8615

Complete contact information is available at: https://pubs.acs.org/10.1021/acs.jctc.3c01179

Notes

The authors declare no competing financial interest.

ACKNOWLEDGMENTS

The authors acknowledge funding from NSF grant OIA-1757220, NASA grant NNH22ZHA004C, and the University of Mississippi's College of Liberal Arts. Additionally, N.R.G. acknowledges the Barry Goldwater Scholarship and Excellence in Education Foundation as well as NSF grant CHE-2150352. The computations for this work were performed at the Mississippi Center for Supercomputing Research. M.C.D. acknowledges the Laboratory Directed Research and Development program of Los Alamos National Laboratory under project no. 20230065DR. M.C.D. also thanks the Center for Nonlinear Studies at LANL for financial support under project no. 20220546CR-NLS.

REFERENCES

- (1) Fortenberry, R. C.; Bodewits, D.; Pierce, D. M. Knowledge Gaps in the Cometary Spectra of Oxygen-bearing Molecular Cations. *Astrophys. J., Suppl. Ser.* **2021**, 256, 6.
- (2) An Updated Fluorescence Emission Model of CO+ for Cometary Science. *Mon. Not. R. Astron. Soc.*, 2024, accepted.
- (3) Zapata Trujillo, J. C.; Pettyjohn, M. M.; McKemmish, L. K. High-Throughput Quantum Chemistry: Empowering the Search for Molecular Candidates behind Unknown Spectral Signatures in Exoplanetary Atmospheres. *Mon. Not. R. Astron. Soc.* **2023**, 524, 361–376.
- (4) Barone, V.; Biczysko, M.; Puzzarini, C. Quantum Chemistry Meets Spectroscopy for Astrochemistry: Increasing Complexity toward Prebiotic Molecules. *Acc. Chem. Res.* **2015**, *48*, 1413–1422.
- (5) Puzzarini, C.; Barone, V. Diving for Accurate Structures in the Ocean of Molecular Systems with the Help of Spectroscopy and Quantum Chemistry. *Acc. Chem. Res.* **2018**, *51*, 548–556.
- (6) Fortenberry, R. C.; Lee, T. J. Computational Vibrational Spectroscopy for the Detection of Molecules in Space. *Annu. Rep. Comput. Chem.* **2019**, *15*, 173–202.
- (7) Gardner, M. B.; Westbrook, B. R.; Fortenberry, R. C.; Lee, T. J. Highly-Accurate Quartic Force Fields for the Prediction of Anharmonic Rotational Constants and Fundamental Vibrational Frequencies. *Spectrochim. Acta, Part A* **2021**, 248, 119184.
- (8) Watrous, A. G.; Westbrook, B. R.; Fortenberry, R. C. F12-TZ-cCR: A Methodology for Faster and Still Highly Accurate Quartic Force Fields. *J. Phys. Chem. A* **2021**, *125*, 10532–10540.
- (9) Fortenberry, R. C.; Lee, T. J. Bowman, J. M., Ed.; World Scientific: Singapore, 2022, pp 235–295. Vibrational Dynamics of Molecules
- (10) Raghavachari, K.; Trucks, G. W.; Pople, J. A.; Head-Gordon, M. A Fifth-Order Perturbation Comparison of Electron Correlation Theories. *Chem. Phys. Lett.* **1989**, *157*, 479–483.
- (11) Helgaker, T.; Ruden, T. A.; Jørgensen, P.; Olsen, J.; Klopper, W. A Priori Calculation of Molecular Properties to Chemical Accuracy. J. Phys. Org. Chem. 2004, 17, 913–933.
- (12) Stanton, J. F.; Bartlett, R. J. The Equation of Motion Coupled-Cluster Method A Systematic Biorthogonal Approach to Molecular Excitation Energies, Transition-Probabilities, and Excited-State Properties. J. Chem. Phys. 1993, 98, 7029–7039.
- (13) Tajti, A.; Stanton, J. F.; Matthews, D. A.; Szalay, P. G. Accuracy of Coupled Cluster Excited State Potential Energy Surfaces. *J. Chem. Theory Comput.* **2018**, *14*, 5859–5869.
- (14) Christiansen, O.; Koch, H.; Jo/rgensen, P. Response functions in the CC3 iterative triple excitation model. *J. Chem. Phys.* **1995**, *103*, 7429–7441.
- (15) Koch, H.; Christiansen, O.; Jo/rgensen, P.; Sanchez de Merás, A. M.; Helgaker, T. The CC3Model: An Iterative Coupled Cluster Approach including Connected Triples. *J. Chem. Phys.* **1997**, *106*, 1808–1818.
- (16) Smith, C. E.; King, R. A.; Crawford, T. D. Coupled cluster methods including triple excitations for excited states of radicals. *J. Chem. Phys.* **2005**, *122*, 054110.

- (17) Loos, P.-F.; Scemama, A.; Jacquemin, D. The Quest for Highly Accurate Excitation Energies: A Computational Perspective. *J. Phys. Chem. Lett.* **2020**, *11*, 2374–2383.
- (18) Watson, T. J.; Lotrich, V. F.; Szalay, P. G.; Perera, A.; Bartlett, R. Benchmarking for Perturbative Triple-Excitations in EE-EOM-CC Methods. *J. Phys. Chem. A* **2013**, *117*, 2569–2579.
- (19) Matthews, D. A.; Stanton, J. F. A New Approach to Approximate Equation-of-Motion Coupled Cluster with Triple Excitations. *J. Chem. Phys.* **2016**, *145*, 124102.
- (20) Agbaglo, D. A.; Cheng, Q.; Fortenberry, R. C.; Stanton, J. F.; DeYonker, N. J. Theoretical Rovibrational Spectroscopy of Magnesium Tricarbide—Multireference Character Thwarts a Full Analysis of All Isomers. *J. Phys. Chem. A* **2022**, *126*, 4132–4146.
- (21) Fortenberry, R. C.; King, R. A.; Stanton, J. F.; Crawford, T. D. A Benchmark Study of the Vertical Electronic Spectra of the Linear Chain Radicals C₂H and C₄H. *J. Chem. Phys.* **2010**, *132*, 144303.
- (22) Morgan, W. J.; Fortenberry, R. C. Quartic Force Fields for Excited Electronic States: Rovibronic Reference Data for the 1 ²A' and 1 ²A'' States of the Isoformyl Radical, HOC. *Spectrochim. Acta, Part A* **2015**, 135, 965–972.
- (23) Morgan, W. J.; Fortenberry, R. C. Theoretical Rovibronic Treatment of the $X \sim 2\Sigma + \text{and } \hat{A}$ 2 Π States of C_2H & \hat{X} 1 $\hat{\Sigma} + \text{State}$ of C_2H^- from Quartic Force Fields. *J. Phys. Chem. A* **2015**, *119*, 7013–7025.
- (24) Davis, M. C.; Fortenberry, R. C. (T)+EOM Quartic Force Fields for Theoretical Vibrational Spectroscopy of Electronically Excited States. *J. Chem. Theory Comput.* **2021**, *17*, 4374–4382.
- (25) Davis, M. C.; Garrett, N. R.; Fortenberry, R. C. F12+EOM Quartic Force Fields for Rovibrational Predictions of Electronically Excited States. *J. Phys. Chem. A* **2023**, *127*, 4771–4779.
- (26) Musiał, M.; Kowalska, K.; Bartlett, R. J. Accurate Calculation of Vibrational Frequencies in Excited States with the Full EOM-CCSDT Method. *J. Mol. Struct.* **2006**, *768*, 103–109.
- (27) Davis, M. C.; Huang, X.; Fortenberry, R. C. Complete, Theoretical Rovibronic Spectral Characterization of the Carbon Monoxide, Water, and Formaldehyde Cations. *Molecules* **2023**, 28, 1782
- (28) Győrffy, W.; Werner, H.-J. Analytical Energy Gradients for Explicitly Correlated Wave Functions. II. Explicitly Correlated Coupled Cluster Singles and Doubles with Perturbative Triples Corrections: CCSD(T)-F12. J. Chem. Phys. 2018, 148, 114104.
- (29) Watson, J. K. G. During, J. R., Ed.; Elsevier: Amsterdam, 1977, pp 1–89. Vibrational Spectra and Structure
- (30) Franke, P. R.; Stanton, J. F.; Douberly, G. E. How to VPT2: Accurate and Intuitive Simulations of CH Stretching Infrared Spectra Using VPT2+K with Large Effective Hamiltonian Resonance Treatments. *J. Phys. Chem. A* **2021**, *125*, 1301–1324.
- (31) Rauhut, G.; Hrenar, T. A Combined Variational and Perturbational Study on the Vibrational Spectrum of P₂F₄. *Chem. Phys.* **2008**, 346, 160–166.
- (32) Piccardo, M.; Penocchio, E.; Puzzarini, C.; Biczysko, M.; Barone, V. Semi-Experimental Equilibrium Structure Determinations by Employing B3LYP/SNSD Anharmonic Force Fields: Validation and Application to Semirigid Organic Molecules. *J. Phys. Chem. A* **2015**, *119*, 2058–2082.
- (33) Puzzarini, C. Astronomical Complex Organic Molecules: Quantum Chemistry Meets Rotational Spectroscopy. *Int. J. Quantum Chem.* **2017**, *117*, 129–138.
- (34) Melosso, M.; Bizzocchi, L.; Gazzeh, H.; Tonolo, F.; Guillemin, J.-C.; Alessandrini, S.; Rivilla, V. M.; Dore, L.; Barone, V.; Puzzarini, C. Gas-Phase Identification of (Z)-1,2-ethenediol, A Key Prebiotic Intermediate in the Formose Reaction. *Phys. Chem. Chem. Phys.* **2022**, *58*, 2750–2753.
- (35) Watrous, A. G.; Westbrook, B. R.; Fortenberry, R. C. The Performance of Hybrid and F12*/F12c Explicitly Correlated Coupled Cluster Methods for Use in Anharmonic Vibrational Frequency Computations. *Int. J. Quantum Chem.* **2023**, 123, No. e27225.

- (36) Agbaglo, D.; Fortenberry, R. C. The performance of explicitly correlated methods for the computation of anharmonic vibrational frequencies. *Int. J. Quantum Chem.* **2019**, *119*, No. e25899.
- (37) Agbaglo, D.; Fortenberry, R. C. The Performance of Explicitly Correlated Wavefunctions [CCSD(T)-F12b] in the Computation of Anharmonic Vibrational Frequencies. *Chem. Phys. Lett.* **2019**, 734, 136720.
- (38) Douglas, M.; Kroll, N. M. Quantum Electrodynamical Corrections to the Fine Structure of Helium. *Ann. Phys.* **1974**, 82, 89–155.
- (39) Yang, W. T.; Parr, R. G.; Lee, C. T. Various Functionals for the Kinetic Energy Density of an Atom or Molecule. *Phys. Rev. A* **1986**, 34, 4586–4590.
- (40) Lee, C.; Yang, W. T.; Parr, R. G. Development of the Colle-Salvetti Correlation-Energy Formula into a Functional of the Electron Density. *Phys. Rev. B* **1988**, *37*, 785–789.
- (41) Becke, A. D. Density-Functional Thermochemistry. III. The Role of Exact Exchange. *J. Chem. Phys.* **1993**, *98*, 5648–5652.
- (42) Becke, A. D. A. A new mixing of Hartree–Fock and local density-functional theories. *J. Chem. Phys.* **1993**, *98*, 1372–1377.
- (43) Yanai, T.; Tew, D. P.; Handy, N. C. A new hybrid exchange—correlation functional using the Coulomb-attenuating method (CAM-B3LYP). *Chem. Phys. Lett.* **2004**, *393*, 51–57.
- (44) Adamo, C.; Barone, V. Toward Reliable Density Functional Methods without Adjustable Parameters: The PBE0Model. *J. Chem. Phys.* **1999**, *110*, 6158–6170.
- (45) Chai, J.-D.; Head-Gordon, M. Long-range Corrected Hybrid Density Functionals With Damped Atom-Atom Dispersion Corrections. *Chem. Phys. Phys. Chem.* **2008**, *10*, 6615–6620.
- (46) Dunning, T. H. Gaussian Basis Sets for Use in Correlated Molecular Calculations. I. The Atoms Boron through Neon and Hydrogen. *J. Chem. Phys.* **1989**, *90*, 1007–1023.
- (47) Kendall, R. A.; Dunning, T. H.; Harrison, R. Electron affinities of the first-row atoms revisited. Systematic basis sets and wave functions. *J. Chem. Phys.* **1992**, *96*, 6796–6806.
- (48) Gauss, J.; Lauderdale, W. J.; Stanton, J. F.; Watts, J. D.; Bartlett, R. J. Analytic Energy Gradients for Open-Shell Coupled-Cluster Singles and Doubles (CCSD) Calculations using Restricted Open-Shell Hartree-Fock (ROHF) Reference Functions. *Chem. Phys. Lett.* 1991, 182, 207–215.
- (49) Lauderdale, W. J.; Stanton, J. F.; Gauss, J.; Watts, J. D.; Bartlett, R. J. Many-Body Perturbation Theory with a Restricted Open-Shell Hartree-Fock Reference. *Chem. Phys. Lett.* **1991**, *187*, 21–28.
- (50) Watts, J. D.; Gauss, J.; Bartlett, R. J. Coupled-Cluster Methods with Noniterative Triple Excitations for Restricted Open-Shell Hartree-Fock and Other General Single Determinant Reference Functions. Energies and Analytical Gradients. *J. Chem. Phys.* **1993**, *98*, 8718–8733.
- (51) Werner, H.-J.; Knowles, P. J.; Knizia, G.; Manby, F. R.; Schütz, M.; Celani, P.; Györffy, W.; Kats, D.; Korona, T.; Lindh, R.; Mitrushenkov, A.; Rauhut, G.; Shamasundar, K. R.; Adler, T. B.; Amos, R. D.; Bennie, S. J.; Bernhardsson, A.; Berning, A.; Cooper, D. L.; Deegan, M. J. O.; Dobbyn, A. J.; Eckert, F.; Goll, E.; Hampel, C.; Hesselmann, A.; Hetzer, G.; Hrenar, T.; Jansen, G.; Köppl, C.; Lee, S. J. R.; Liu, Y.; Lloyd, A. W.; Ma, Q.; Mata, R. A.; May, A. J.; McNicholas, S. J.; Meyer, W.; Miller, III, T. F.; Mura, M. E.; Nicklaß, A.; O'Neill, D. P.; Palmieri, P.; Peng, D.; Pflüger, K.; Pitzer, R.; Reiher, M.; Shiozaki, T.; Stoll, H.; Stone, A. J.; Tarroni, R.; Thorsteinsson, T.; Wang, M.; Welborn, M. 2022; see http://www.molpro.net (accessed Sep, 2023).
- (52) Werner, H.-J.; Knowles, P. J.; Knizia, G.; Manby, F. R.; Schütz, M. Molpro: A General-Purpose Quantum Chemistry Program Package. Wiley Interdiscip. Rev.: Comput. Mol. Sci. 2012, 2, 242—253. (53) Frisch, M. J.; Trucks, G. W.; Schlegel, H. B.; Scuseria, G. E.; Robb, M. A.; Cheeseman, J. R.; Scalmani, G.; Barone, V.; Petersson, G. A.; Nakatsuji, H.; Li, X.; Caricato, M.; Marenich, A. V.; Bloino, J.; Janesko, B. G.; Gomperts, R.; Mennucci, B.; Hratchian, H. P.; Ortiz, J. V.; Izmaylov, A. F.; Sonnenberg, J. L.; Williams-Young, D.; Ding, F.; Lipparini, F.; Egidi, F.; Goings, J.; Peng, B.; Petrone, A.; Henderson,

- T.; Ranasinghe, D.; Zakrzewski, V. G.; Gao, J.; Rega, N.; Zheng, G.; Liang, W.; Hada, M.; Ehara, M.; Toyota, K.; Fukuda, R.; Hasegawa, J.; Ishida, M.; Nakajima, T.; Honda, Y.; Kitao, O.; Nakai, H.; Vreven, T.; Throssell, K.; Montgomery, Jr., J. A.; Peralta, J. E.; Ogliaro, F.; Bearpark, M. J.; Heyd, J. J.; Brothers, E. N.; Kudin, K. N.; Staroverov, V. N.; Keith, T. A.; Kobayashi, R.; Normand, J.; Raghavachari, K.; Rendell, A. P.; Burant, J. C.; Iyengar, S. S.; Tomasi, J.; Cossi, M.; Millam, J. M.; Klene, M.; Adamo, C.; Cammi, R.; Ochterski, J. W.; Martin, R. L.; Morokuma, K.; Farkas, O.; Foresman, J. B.; Fox, D. J. Gaussian 16 Revision C.01.; Gaussian Inc: Wallingford CT, 2016.
- (54) Fortenberry, R. C.; Huang, X.; Crawford, T. D.; Lee, T. J. The 1 ³A' HCN and 1 ³A' HCO⁺ Vibrational Frequencies and Spectroscopic Constants from Quartic Force Fields. *J. Phys. Chem.* A **2013**, *117*, 9324–9330.
- (55) Gaw, J. F.; Willets, A.; Green, W. H.; Handy, N. C. Bowman, J. M., Ratner, M. A., Eds.; JAI Press, Inc.: Greenwich, CT, 1991, pp 170–185. Advances in Molecular Vibrations and Collision Dynamics
- (56) Westbrook, B. R.; Fortenberry, R. C. pbQFF: Push-Button Quartic Force Fields. *J. Chem. Theory Comput.* **2023**, *19*, 2606–2615. (57) Tack, L. M.; Rosenbaum, N. H.; Owrutsky, J. C.; Saykally, R. J. Velocity Modulation Infrared Laser Spectroscopy and Structure of the Amide Anion (NH₂⁻). *J. Chem. Phys.* **1986**, *85*, 4222–4227.
- (58) Johns, J. W. C.; McKellar, A. R. W.; Weinberger, E. The Infrared Spectrum of HNO. Can. J. Phys. 1983, 61, 1106–1119.
- (59) Yamada, C.; Endo, Y.; Hirota, E. Difference Frequency Laser Spectroscopy of the ν_1 Band of the HO₂ Radical. *J. Chem. Phys.* **1983**, 78, 4379–4384.
- (60) Chen, J.; Dagdigian, P. J. Spectrally resolved fluorescence in the HNF (DNF) Ã2A' Ã2 A" band system. *Chem. Phys. Lett.* **1993**, 213, 586–592.
- (61) Yoshikawa, T.; Watanabe, A.; Sumiyoshi, Y.; Endo, Y. Laser spectroscopy of the 2A'-2A'' system for the HSO radical. *J. Mol. Spectrosc.* **2009**, 254, 119–125.
- (62) Ashworth, S. H.; Fink, E. H. The High Resolution Fourier-Transform Chemiluminescence Spectrum of the HS₂ Radical. *Mol. Phys.* **2007**, *105*, 715–725.
- (63) Huber, K. P.; Herzberg, G.; Gallagher, J. W.; Johnson, R. D. Linstrom, P. J., Mallard, W. G., Eds.; National Institute of Standards and Technology: Gaithersburg MD, 2018, p 69. Constants of Diatomic Molecules
- (64) Shimanouchi, T. Tables of Molecular Vibrational Frequencies, 39th ed.; National Standards Reference Data System: Washington, DC, 1972; Vol. 1.
- (65) Jacox, M. E. Vibrational and Electronic Energy Levels of Polyatomic Transient Molecules. Supplement B. J. Phys. Chem. Ref. Data 2003, 32, 1–441.
- (66) Amano, T.; Tanaka, K. Difference Frequency Laser Spectroscopy of the ν₁ Band of HOCO⁺. J. Chem. Phys. 1985, 82, 1045–1046.
- (67) Amano, T.; Tanaka, K. Difference Frequency Laser Spectroscopy of the ν_1 Fundamental Band of HOCO⁺. *J. Chem. Phys.* **1985**, 83, 3721–3728.
- (68) Douberly, G. E.; Ricks, A. M.; Ticknor, B. W.; Duncan, M. A. Structure of Protonated Carbon Dioxide Clusters: Infrared Photodissociation Spectroscopy and ab Initio Calculations. *J. Phys. Chem. A* **2008**, *112*, 950–959.
- (69) Burkholder, J. B.; Hammer, P. D.; Howard, C. J.; Towle, J. P.; Brown, J. M. Fourier Transform Spectroscopy of the ν_2 and ν_3 Bands of HO₂. *J. Mol. Spectrosc.* **1992**, *151*, 493–512.
- (70) Lindsay, D. M.; Gole, J. L.; Lombardi, J. R. An analysis of the hydrazine—fluorine flame. The 2A'-2A]" emission spectrum of HNF and its relation to other HAB co. *Chem. Phys.* **1979**, *37*, 333–342.
- (71) Brünken, S.; Müller, H. S. P.; Lewen, F.; Winnewisser, G. High Accuracy Measurements on the Ground State Rotational Spectrum of Formaldehyde ($\rm H_2CO$) up to 2 THz. *Phys. Chem. Chem. Phys.* **2003**, 5, 1515–1518.
- (72) Bancroft, J. L.; Hollas, J. M.; Ramsay, D. A. The Absorption Spectra of HNO and DNO. *Can. J. Phys.* **1962**, *40*, 322–347.
- (73) Dalby, F. W. The Spectrum and Structure of the HNO Molecule. Can. J. Phys. 1958, 36, 1336–1371.

- (74) Fink, E. H.; Kruse, H.; Ramsay, D. A. Paper WF2, 42nd Symposium on Molecular Spectroscopy; Ohio State University, 1987.
- (75) Hunziker, H. E.; Wendt, H. R. Electronic Absorption Spectra of Organic Peroxyl Radicals in the Near Infrared. *J. Chem. Phys.* **1976**, 64, 3488–3490.
- (76) Becker, K.; Fink, E.; Leiss, A.; Schurath, U. A Study of the Near Infrared Emission Bands of the Hydroperoxyl Radical at Medium Resolution. *Chem. Phys. Lett.* **1978**, *54*, 191–196.
- (77) Woodman, C. M. The Absorption Spectrum of HNF in the Region 3800–5000 Å. J. Mol. Spectrosc. 1970, 33, 311–344.
- (78) Schurath, U.; Weber, M.; Becker, K. H. Electronic Spectrum and Structure of the HSO Radical. *J. Chem. Phys.* **1977**, *67*, 110–119.
- (79) Entfellner, M.; Boesl, U. Photodetachment-Photoelectron Spectroscopy of Disulfanide: the Ground and First Excited Electronic State of HS₂ and DS₂. *Phys. Chem. Chem. Phys.* **2009**, *11*, 2657.
- (80) Job, V.; Sethuraman, V.; Innes, K. The 3500 Å $1A_2$ - $X\sim^1A_1$ Transition of Formaldehyde- H_2 , D_2 , and HD: Vibrational and Rotational Analyses. *J. Mol. Spectrosc.* **1969**, 30, 365–426.
- (81) Clouthier, D. J.; Ramsay, D. A. The Spectroscopy of Formaldehyde and Thioformaldehyde. *Annu. Rev. Phys. Chem.* **1983**, 34, 31–58.
- (82) Moule, D. C.; Walsh, A. D. Ultraviolet Spectra and Excited States of Formaldehyde. *Chem. Rev.* 1975, 75, 67–84.
- (83) Del Bene, J. E.; Gwaltney, S. R.; Bartlett, R. J. Base Properties of Hi₂CO in the Excited $^1n \rightarrow \pi^*$ State. *J. Phys. Chem. A* **1998**, 102, 5124–5127.
- (84) Bonfanti, M.; Petersen, J.; Eisenbrandt, P.; Burghardt, I.; Pollak, E. Computation of the $S_1 \leftarrow S_0$ Vibronic Absorption Spectrum of Formaldehyde by Variational Gaussian Wavepacket and Semiclassical IVR Methods. J. Chem. Theory Comput. **2018**, 14, 5310–5323.
- (85) Fortenberry, R. C.; Huang, X.; Francisco, J. S.; Crawford, T. D.; Lee, T. J. Quartic Force Field Predictions of the Fundamental Vibrational Frequencies and Spectroscopic Constants of the Cations HOCO⁺ and DOCO⁺. *J. Chem. Phys.* **2012**, *136*, 234309.
- (86) Huang, X.; Fortenberry, R. C.; Lee, T. J. Protonated Nitrous Oxide, NNOH⁺: Fundamental Vibrational Frequencies and Spectroscopic Constants from Quartic Force Fields. *J. Chem. Phys.* **2013**, *139*, 084313.
- (87) Kitchens, M. J. R.; Fortenberry, R. C. The Rovibrational Nature of Closed-Shell Third-Row Triatomics: HOX and HXO, X = Si⁺, P, S⁺, and Cl. *Chem. Phys.* **2016**, 472, 119–127.
- (88) Bieler, A.; Altwegg, K.; Balsiger, H.; Bar-Nun, A.; Berthelier, J.-J.; Bochsler, P.; Briois, C.; Calmonte, U.; Combi, M.; De Keyser, J.; van Dishoeck, E. F.; Fiethe, B.; Fuselier, S. A.; Gasc, S.; Gombosi, T. I.; Hansen, K. C.; Hässig, M.; Jäckel, A.; Kopp, E.; Korth, A.; Le Roy, L.; Mall, U.; Maggiolo, R.; Marty, B.; Mousis, O.; Owen, T.; Rème, H.; Rubin, M.; Sémon, T.; Tzou, C.-Y.; Waite, J. H.; Walsh, C.; Wurz, P. Abundant Molecular Oxygen in the Coma of Comet 67P/Churyumov–Gerasimenko. *Nature* 2015, 526, 678–681.
- (89) Filacchione, G.; Sanctis, M. C. D.; Capaccioni, F.; Raponi, A.; Tosi, F.; Ciarniello, M.; Cerroni, P.; Piccioni, G.; Capria, M. T.; Palomba, E.; Bellucci, G.; Erard, S.; Bockelee-Morvan, D.; Leyrat, C.; Arnold, G.; Barucci, M. A.; Fulchignoni, M.; Schmitt, B.; Quirico, E.; Jaumann, R.; Stephan, K.; Longobardo, A.; Mennella, V.; Migliorini, A.; Ammannito, E.; Benkhoff, J.; Bibring, J. P.; Blanco, A.; Blecka, M. I.; Carlson, R.; Carsenty, U.; Colangeli, L.; Combes, M.; Combi, M.; Crovisier, J.; Drossart, P.; Encrenaz, T.; Federico, C.; Fink, U.; Fonti, S.; Ip, W. H.; Irwin, P.; Kuehrt, E.; Langevin, Y.; Magni, G.; McCord, T.; Moroz, L.; Mottola, S.; Orofino, V.; Schade, U.; Taylor, F.; Tiphene, D.; Tozzi, G. P.; Beck, P.; Biver, N.; Bonal, L.; Combe, J.-P.; Despan, D.; Flamini, E.; Formisano, M.; Fornasier, S.; Frigeri, A.; Grassi, D.; Gudipati, M. S.; Kappel, D.; Mancarella, F.; Markus, K.; Merlin, F.; Orosei, R.; Rinaldi, G.; Cartacci, M.; Cicchetti, A.; Giuppi, S.; Hello, Y.; Henry, F.; Jacquinod, S.; Reess, J. M.; Noschese, R.; Politi, R.; Peter, G. Exposed water ice on the nucleus of comet 67P/ Churyumov-Gerasimenko. Nature 2016, 529, 368-374.